universe

MDPI

Article

Measuring the Casimir Forces with an Adhered Cantilever: Analysis of Roughness and Background Effects

Ivan A. Soldatenkov [1,†], Anastasiya A. Yakovenko [1] and Vitaly B. Svetovoy [2,*,†]

[1] Ishlinsky Institute for Problems in Mechanics, Russian Academy of Sciences, Prospect Vernadskogo, 101-1, 119526 Moscow, Russia; isoldat@mail.ru (I.A.S.); anastasiya.yakovenko@phystech.edu (A.A.Y.)
[2] A. N. Frumkin Institute of Physical Chemistry and Electrochemistry, Russian Academy of Sciences, Leninsky Prospect 31 Bld. 4, 119071 Moscow, Russia
* Correspondence: svetovoy@yandex.ru
† These authors contributed equally to this work.

Abstract: Technological progress has made possible precise measurements of the Casimir forces at distances less than 100 nm. It has enabled stronger constraints on the non-Newtonian forces at short separations and improved control of micromechanical devices. Experimental information on the forces below 30 nm is sparse and not precise due to pull-in instability and surface roughness. Recently, a method of adhered cantilever was proposed to measure the forces at small distances, which does not suffer from the pull-in instability. Deviation of the cantilever from a classic shape carries information on the forces acting nearby the adhered end. We calculate the force between a flat cantilever and rough Au plate and demonstrate that the effect of roughness dominates when the bodies approach the contact. Short-distance repulsion operating at the contact is included in the analysis. Deviations from the classic shape due to residual stress, inhomogeneous thickness of the cantilever, and finite compliance of the substrate are analysed. It is found that a realistic residual stress gives a negligible contribution to the shape, while the finite compliance and inhomogeneous thickness give measurable contributions that have to be subtracted from the raw data.

Keywords: Casimir forces; non-Newtonian forces; short distances; surface roughness; adhered cantilever; contact mechanics; elastic beam

check for updates

Citation: Soldatenkov, I.A.; Yakovenko, A.A.; Svetovoy, V.B. Measuring the Casimir Forces with an Adhered Cantilever: Analysis of Roughness and Background Effects. *Universe* **2021**, *7*, 64. https://doi.org/10.3390/universe7030064

Academic Editor: Galina L. Klimchitskaya

Received: 18 February 2021
Accepted: 9 March 2021
Published: 10 March 2021

Publisher's Note: MDPI stays neutral with regard to jurisdictional claims in published maps and institutional affiliations.

Copyright: © 2021 by the authors. Licensee MDPI, Basel, Switzerland. This article is an open access article distributed under the terms and conditions of the Creative Commons Attribution (CC BY) license (https://creativecommons.org/licenses/by/4.0/).

1. Introduction

Quantum fluctuations of the electromagnetic field manifest themselves in very different physical circumstances such as sticking gecko to walls or evaporation of black holes. Van der Waals (vdW) attraction between nonpolar molecules is also the effect of quantum fluctuations as was explained by London [1]. With the increase of the distance the attractive forces decrease faster than the vdW interaction due to the retardation of electromagnetic field as was demonstrated by Casimir and Polder [2]. The same interaction results in an attractive force between parallel plates separated by a short distance. This force, which is called the Casimir force (CF), was deduced between perfect mirrors by applying the zero-field boundary condition on the plates [3]. If the plates are separated by the distance h, the force per unit area is given by a surprisingly simple expression

$$P_C(h) = \frac{\pi^2 \hbar c}{240 h^4}, \tag{1}$$

where only the fundamental constants $\hbar$ and c enter the formula. Lifshitz and coworkers [4,5] proposed a united theory that reproduces all the separate results as different limit cases. The theory takes into account realistic dielectric properties of interacting materials and accounts not only for quantum but also for thermal fluctuations. In the heart of this theory lies the fluctuation–dissipation theorem.

Casimir forces are the subject of active investigation in the last 20 years (see, for example, the reviews [6–8]). The modern technological level is high enough to control separations of the order of 100 nm and made possible precise measurements of the forces [9–18]. The interest in the forces is related to their role in micro/nanoelectromechanical systems (MEMS/NEMS). These systems have elements with a sufficiently large area separated by a sufficiently small distance to allow the CF to become operative [19–25]. On the other hand, precise measurement of the CF allows us to make constraints on the forces beyond Newtonian gravity at short separations. The better we know the CF the stronger we can restrict new physics beyond the standard model. For distances larger than 10 μm the strongest constraints on the non-Newtonian gravity follow from Cavendish-type experiments [26,27] but at distances smaller than a few micrometers the strongest restrictions on the hypothetical forces follow from the Casimir-type experiments [28–30] (see also a recent comprehensive review [31]). For separations smaller than 10 nm the strongest constraints follow from the experiments on neutron scattering [32–34].

The CF have been measured with a high precision of the order of 1% in the distance range from 62 nm [10] up to 1 μm [18]. It is difficult to do measurements with a similar precision at shorter separations. Uncertainty in the force is dominated by the error in the absolute distance h, which for all the experiments is $\Delta h \sim 1$ nm. The corresponding relative error in the force is $\Delta P_C / P_C = \alpha \Delta h / h$, where $3 < \alpha < 4$ and the force behaves as $\sim h^{-\alpha}$. Obviously the error in the force will increase with the decrease of the separation. Moreover, at short separations an additional problem occurs. All systems used to measure the forces employ the elastic suspension (torsional pendulum or cantilever with a ball attached) that loses stability at sufficiently short separations. This is a generic feature of the elastic suspension. Practically, it was possible to go down to $h = 12$ nm [35] in measuring the force with an atomic force microscope (AFM) between a sphere and plate covered with gold. Stiff cantilevers were used for that and the measurement precision was not high. The surface force apparatus that uses much stiffer springs is more stable, but even in this case the smallest distance in vacuum was about 8.5 nm [36]. The measurements at these short separations are sparse [35–37] and have low precision.

Besides the loss of stability an important factor at short separations is the surface roughness. The Lifshitz theory predicts the forces between flat surfaces but in reality all surfaces are rough and the effect of roughness becomes important at distances considerably larger than the root-mean-square (rms) roughness w. For gold films thermally evaporated on Si substrates it was established experimentally [38] that roughness influences significantly the CF between a sphere and plate at distances $h \lesssim 7w$. In this range the forces strongly deviate from the expected regime $\sim h^{-\alpha}$. The effect has been explained by the presence of high rare peaks on the rough surface, which can approach very close to the opposite body and give significant contribution to the force [39,40].

Thus, the CF at distances below 30 nm are poorly investigated due to instability of elastic suspensions and due to roughness effects when the bodies approach the contact. Recently an experiment has been proposed [41] allowing exploration of the distance range from 5 nm to 30 nm. Instead of the elastic suspension it is proposed to use an adhered cantilever to measure the forces. Such a cantilever is a rectangular flexible beam, one end of which is firmly fixed at a height H above a substrate and the other end is adhered to the substrate mainly due to vdW-Casimir forces. The shape of the cantilever was shown to be sensitive to the forces acting nearby the adhered end [42] with the maximum effect at 1/3 of its unadhered length. The main advantages of the adhered cantilever method are the following: (a) In contrast to the elastic suspension the adhered cantilever never losses stability (no pull-in instability at short distances). For this reason it can be used to measure the forces at short distances. (b) The force and the adhesion energy are measured simultaneously. (c) The force is measured between practically parallel surfaces. No restrictions exist on the interaction area as for the standard sphere-plate configuration. However, there is a disadvantage of the method. It is not possible to change freely the distance, at which the force is measured. Each measurement gives the force at the distance

h_0 that is defined as the average distance between rough bodies at contact. To change the distance one has to change the roughness of contacting surfaces that can be realised only by fabrication of new surfaces.

If no force is acting outside of the adhered area, the cantilever takes a classic shape that is well defined within the theory of elasticity. The interaction between the cantilever and substrate will change the shape and the deviation from the classic shape is the value that is measured in the proposed experiment. However, there are a few effects (background effects), which provide small corrections to the classic shape independently on the measured forces, that have to be taken into account. The effects are the following. (i) The cantilevers are characterised by a residual stress, which results to their initial (before adhesion) bending. (ii) Thickness of the cantilever is not completely homogeneous, which can change slightly the classic shape. (iii) The adhered end sticks to the substrate, which is not absolutely stiff. A finite compliance of the substrate also can result in the correction to the classic shape.

Accounting for the finite compliance of the substrate requires consideration of the contact problem that includes intermolecular interactions. In contact mechanics these interactions were taken into account for the first time in relation to the Hertz contact [43]. Many effective approaches to the contact problem were developed including contact between solids with surface roughness (see, for example, [44]). In particular, a continual model of the surface roughness as a deformable layer was proposed, where compliance is described by the Winkler model (nonlinear in general) [45,46]. Description for the contact interaction between cantilever and substrate in the unadhered area requires the use of a self-consistent approach (according to Derjaguin) [47]. Such an approach implies that a gap between solids in contact ensures the balance between deformation and intermolecular forces on the interface. Self-consistent approach was applied to the contact problems for solids with a Winkler type layer [48,49].

In this paper we discuss the CF between the cantilever and substrate that differ from those predicted by the Lifshitz theory because of the effect of roughness and analyse how these additional contributions influence the shape of the cantilever. To be able to extract information on the CF from the experiment we also analyse the influence of the background effects on the classic shape of the cantilever. It includes the residual stress in the cantilever, inhomogeneous thickness of the cantilever, and finite compliance of the substrate in the adhered area.

2. Method of Adhered Cantilever

First, let us define the terminology used in this paper. At very short distances the fluctuation induced forces between bulk bodies decreasing with the distance as h^{-3} are called the vdW forces, while at larger separations the forces behave as h^{-4} and are called the Casimir forces. There is no physical difference in the origin of these forces, just in the first case (vdW forces) retardation of the electromagnetic signal is neglected, but in the second case (CF) it is fully taken into account. We consider here the transition region but continue to call the forces conditionally the Casimir forces even in the vdW limit. Since relatively short distances are considered, we neglect the thermal fluctuations, which play a significant role at much larger distances $h \sim \hbar c/2T = 3.8$ μm where T is the temperature in energy units.

In this section we briefly describe the idea of the method [41] that allows measuring the forces at distances close to contact. In the process of fabrication or operation of MEMS separate elements can stick together that result in malfunction of the entire device [50–52]. To investigate the effect of the irreversible stiction, a model system was proposed that is the adhered cantilever shown in Figure 1. The cantilever sticks to a substrate (typically silicon) covered with a functional layer, which is a material with a certain roughness. The total length of the cantilever is L and the unadhered length is s. It is assumed that in the adhered range with the length $L - s$ the adhesion energy per unit area is Γ.

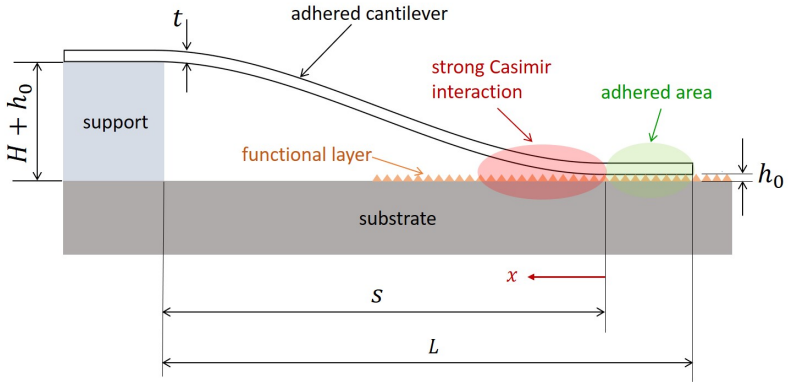


Figure 1. Adhered cantilever. The main geometric characteristics are shown. Average distance at contact h_0 is defined by the roughness of the functional layer. Realistic roughness is presented schematically by brown triangles. Areas of adhesion and strong CF are highlighted.

If we neglect the Casimir interaction near the adhered end, the deflection of the cantilever is described by the classic shape

$$u_0(x) = H(1 - 3\xi^2 + 2\xi^3), \quad \xi = x/s \tag{2}$$

that is defined by the minimum of the elastic energy of the beam with the boundary conditions $u_0(0) = H$, $u_0'(0) = 0$ and $u_0(s) = 0, u_0'(s) = 0$. The unadhered length s is related to the adhesion energy Γ by the classic relation [53]

$$\Gamma = \frac{3Et^3H^2}{2s^4}, \tag{3}$$

where E is the Young modulus of the cantilever material and the height H and thickness t are shown in Figure 1. This relation has been used to determine experimentally the value of Γ. In reality the Casimir interaction cannot be completely neglected since it is always strong in the area close to the adhered end. Near this end the average distance between the cantilever and substrate approaches the value h_0. This distance is defined by roughness of the contacting bodies and in the planned experiment the value will be varied in the range $5 < h_0 < 30$ nm. Influence of the CF on the shape of the cantilever was analysed by modelling the force with the following dependence [42]

$$P_C(h) = P_0(h_0/h)^\alpha, \quad P_0 = P_C(h_0) \tag{4}$$

that is a good approximation for the force given by the Lifshitz theory in a restricted range of distances between flat parallel plates. For the configuration of adhered cantilever the running distance is $h = H - u(x) + h_0$.

Influence of the CF (4) on the shape of the cantilever is shown in Figure 2. The important parameters are the following:

$$R = H/h_0 \gg 1, \quad K = (P_0/P_s)^{1/4}, \quad P_s = \frac{Et^3H}{12s^4}, \tag{5}$$

where P_s is an equivalent of the elastic pressure. The figure shows the absolute deviation $u(x) - u_0(x)$ from the classic shape as a function of x-coordinate along the beam. One can see that the maximum deviation from $u_0(x)$ is realised at $x = s/3$ and the deviation strongly depends on the parameter K. When K approaches the critical value $K_c \sim R^{1/4}$ the deviation reaches the absolute maximum that scales as $R^{-1/2}$. The experiment has to be designed in such a way that K is as close to K_c as possible. In this case the deviation from the classic shape can be as large as a few percents that is well measurable with interferometric methods (see details in [41]).

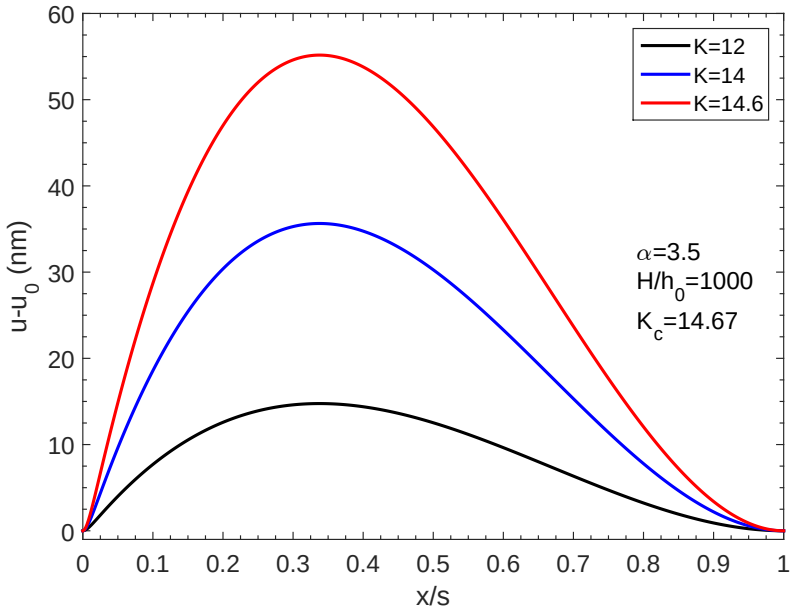


Figure 2. Contribution of the CF to the shape of the cantilever. The difference from the classic shape is shown as a function of normalised coordinate $\xi = x/s$ for $H = 10$ μm. Note that the origin of x-coordinate is at the adhered end. The results are presented for a few values of the parameter K.

The dependencies described above correspond to an ideal situation. In the real world the force between the cantilever and substrate does not follow Equation (4) even approximately. This is because the surface roughness gives significant contribution to the force at short distances. Besides this, one can expect appreciable contributions to the classic shape from the residual stress in the cantilever, nonhomogeneous thickness of the cantilever, and finite compliance of the substrate. All these effects have to be taken into account to extract reliable values of the force from the experiment. These effects are discussed below.

To determine the contribution to the shape of the cantilever, many parameters characterising the problem will be used in this paper. These parameters are related to the geometrical characteristics of the cantilever, describe roughness of deposited Au films, optical properties of materials, or mechanical properties of the solids in contact. The most important parameters are defined in Table 1, where their expected values are presented together with the references for more detailed information.

Table 1. Main parameters describing the adhered cantilever and material properties related to the force measurements.

Parameters	Definition	Value	Refs.
geometrical			[41]
L	total length of the cantilever	5–10 mm	
s	unadhered length of the cantilever	3–5 mm	
t	thickness of the cantilever	10 μm	
H	height of the support	10 μm	
roughness (Au)			[39,40,54]
w	root-mean-square roughness	$1-5$ nm	
l_a	correlation length	30–50 nm	
A	parameter describing high peaks	∼1	
B	parameter describing high peaks	0.05–0.2 nm^{-1}	
optical (Au)			[55]
ω_p	plasma frequency	7.84 eV	
γ	relaxation frequency	49 meV	

Table 1. *Cont.*

Parameters	Definition	Value	Refs.
mechanical			
E	Young modulus	160 GPa (Si), 78 GPa (Au)	
P_f	plasticity limit	0.25 GPa (Au)	[56]
Γ	adhesion energy	10–1000 $\mu J/m^2$	[53]
h_0	average separation at contact	$\sim$10 nm	[35]
h_c	minimum distance between solids	$\approx$0.3 nm	[57]

3. Interaction between the Cantilever and Rough Substrate

Let us consider the simplest realisation of the experiment when a very smooth and stiff cantilever made of silicon single crystal with a typical rms roughness of 0.3 nm interacts with Si substrate covered by a softer metallic layer (functional layer) sputtered or thermally deposited on the substrate. It is assumed that the rms roughness of the metallic layer is considerably larger. Therefore, we will analyse the force between a flat and stiff silicon surface and a rough deformable metal as a function of the average distance h, which can be smaller than the highest roughness peaks. For any position along the cantilever this force consists of three contribution: the CF between flat surfaces separated by the average distance h, correction to the force between flat surfaces that appears due to roughness of the metallic surface $P_{rough}(h)$, and the force that originates from the contact between some asperities and the flat Si surface $P_{cont}(h)$:

$$P_C(h) = P_L(h) + P_{rough}(h) + P_{cont}(h), \tag{6}$$

where the first term $P_L(h)$ is calculated within the Lifshitz theory. The last term needs special attention that is going beyond the scope of this paper. Its contribution is not necessary small in the adhered area at $h = h_0$ but decreases very fast with h increase in the unadhered area. However, our purpose here is to see the influence of the deviations from the Lifshitz contribution on the shape of the cantilever. This effect can be well analysed only with $P_{rough}(h)$. Moreover, it has to be noted that the contact term is exactly zero in the limit of zero load (small adhesion energy).

3.1. Lifshitz Contribution

The first contribution in Equation (6) is the standard term that is given by the Lifshitz formula [5]. It is well-known and presented here only for completeness. Since we consider rather short separations $h < 50$ nm one can change the summation over discrete Matsubara frequencies by the integral over all imaginary frequencies. This approximation means that we neglect all thermal fluctuations that are justified at short separations. We use here a representation of the Lifshitz formula [58], which is convenient due to fast convergence of the integrals:

$$P_L(h) = \frac{\hbar c}{32\pi^2 h^4} \sum_{\nu=s,p} \int_0^1 dt \int_0^\infty dx x^3 \frac{r_1^\nu r_2^\nu e^{-x}}{1 - r_1^\nu r_2^\nu e^{-x}}, \tag{7}$$

where the variables of integration are expressed via the physical quantities as $x = 2h(\zeta^2/c^2 + q^2)^{1/2}$, $tx = 2h\zeta/c$ (ζ is the imaginary frequency and q is the magnitude of the wave vector directed along the plate). In this representation the Fresnel reflection coefficients r_i^ν ($i = 1, 2$ enumerates the bodies) for two possible polarizations $\nu = s, p$ can be written as

$$r_i^s = \frac{1 - \sqrt{1 + t^2(\varepsilon_i - \varepsilon_0)}}{1 + \sqrt{1 + t^2(\varepsilon_i - \varepsilon_0)}}, \quad r_i^p = \frac{\varepsilon_i - \varepsilon_0\sqrt{1 + t^2(\varepsilon_i - \varepsilon_0)}}{\varepsilon_i + \varepsilon_0\sqrt{1 + t^2(\varepsilon_i - \varepsilon_0)}}. \tag{8}$$

Here ε_i and ε_0 are the dielectric functions of the plates and intervening medium. All these functions have to be taken at the imaginary frequencies $\zeta = txc/2h$. The functions at

imaginary frequencies can be expressed via the directly measurable dielectric functions at real frequencies with the Kramers–Kronig relation

$$\varepsilon(i\zeta) = 1 + \frac{2}{\pi}\int_0^\infty d\omega \frac{\omega\varepsilon''(\omega)}{\omega^2+\zeta^2}, \tag{9}$$

where $\varepsilon''(\omega)$ is the imaginary part of the corresponding dielectric function.

3.2. Roughness Contribution

In genal case the roughness contribution to the force is a difficult problem especially at short separations when the roughness amplitude is comparable with the distance between the bodies. The problem is related to the nonadditivity of the CF. At distances large in comparison with the rms roughness there is a well defined procedure to calculate the roughness contribution perturbatively [59,60]. However, the perturbation theory is broken long before the bodies approach the contact as follows form the experimental data [38]. A way to calculate the roughness contribution, while the bodies did not get into contact, was proposed in Refs. [39,40]. The approach is based on the separation of normal asperities (height $\sim w$) and high peaks $> 3w$. The first are accounted perturbatively but the contribution of the high peaks can be calculated additively since the peaks are rare. However, we consider small distances, when a typical lateral size of asperities (the correlation length l_a) is comparable or larger than the separation distance $l_a \gtrsim h$. In this situation all asperities can be accounted additively [59].

It is rather simple to calculate the roughness contribution additively: we have to take the sum over all asperities, which height is smaller than the distance between the bodies. Mathematically it can be expressed as

$$P_{rough}(h) = \int_{-h_1}^{h_0-h_c} dz f(z)[P(h-z) - P(h)]. \tag{10}$$

Here $f(z)$ is the probability density function to find an asperity with the height z and $P(h)$ nearly coincides with $P_L(h)$ except for very small h (see below). The upper integration limit is smaller than the average distance between bodies at contact h_0 on a very small value $h_c \ll h_0$ that has the meaning of an equilibrium distance at contact as explained below. In the lower integration limit the value h_1 is the deepest pit in the roughness profile. Because the force at the distance $h + h_1$ is significantly smaller than that at h and $f(-h_1) \ll 1$ we can safely put $h_1 \to \infty$. Typical value of h_0 is larger than $3w$ and on the upper limit $f(h_0 - h_c) \ll 1$. It means that the second term in Equation (10) is practically equal to the Lifshitz contribution and (10) presents a pure roughness correction in the total force.

The argument in $P(h-z)$ can be very close to zero at the upper integration limit. This is the reason why $P(h)$ has to differ from $P_L(h)$: the force has to stay finite when the argument is going to zero. The physical reason for the modification of $P_L(h)$ at very short separations (angstrom range) is the repulsion of electron clouds so that the equilibrium distance between the bodies cannot be zero. The modification is important only at separations close to contact. We parameterise $P(h)$ as

$$P(h) = P_L(h)\left[1 - (h_c/h)^6\right], \tag{11}$$

where h_c is the equilibrium distance at contact without external load, which is in the range 0.2–0.3 nm. This parametrization follows from the Lennard-Jones potential between molecules 1 and 2 that has the standard form:

$$U_{LJ} = 4E_{0ij}\left[\left(\sigma_{ij}/r_{ij}\right)^6 - \left(\sigma_{ij}/r_{ij}\right)^{12}\right], \tag{12}$$

where r_{ij} is the distance between the molecules i and j and E_{0ij} and σ_{ij} are the corresponding parameters. If we calculate additively with the potential (12) the interaction energy between two parallel plates made of molecules $i = 1$ and $j = 2$, then this energy can be presented as

$$\mathcal{U}(h) = \frac{A_H}{12\pi h^2}\left[1 - \frac{1}{4}\left(\frac{h_c}{h}\right)^6\right], \tag{13}$$

where A_H is the Hamaker constant. Both the parameters A_H and h_c are related to the original Lennard-Jones parameters, but for A_H this relation has no special meaning because the vdW forces are not additive. On the contrary, the molecule sizes do not change significantly when the molecules are arranged in a solid and we can relate $h_c = (2/15)^{1/6}\sigma_{12}$. If materials 1 and 2 are different, one can use the standard rule for molecular dynamics: $\sigma_{12} = (\sigma_{11} + \sigma_{22})/2$. When gold interacts with silicon we can take $\sigma_{11} = 0.293$ nm for Au and $\sigma_{22} = 0.392$ nm for Si [61] and find for $h_c = 0.245$ nm.

Information on roughness statistics of the substrate can be collected from AFM images. Since high peaks play a very important role [54], it is necessary to collect information from as large area as possible. For our calculations we use one of the images collected for the paper [54]. It is a 200 nm thick Au film thermally deposited on Si substrate. The image size is 20×20 μm taken with a resolution of 4096 pixels per line. The correlation length is estimated as $l_a \approx 45$ nm and the rms roughness is $w = 2.35$ nm. The height distribution function $f(z)$ extracted from the image is shown in Figure 3. The important feature of this function is that the high peaks are not described by the normal distribution that is shown by the red dashed line. The normal distribution works rather well for the heights in the range $-3w < z < 3w$ but for the high peaks and deep pits is does not describe the statistic of the roughness.

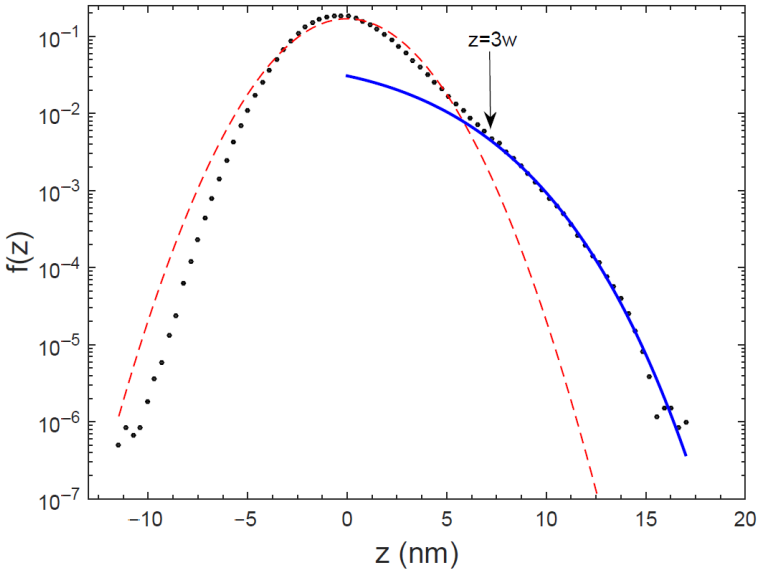


Figure 3. The probability density function as a function of the random height of asperities z. Black circles are the data collected directly from the AFM images, the red dashed curve shows the normal distribution with the same rms roughness, and the blue solid curve demonstrates the extreme value distribution. The last distribution describes well the high peak tail.

Deep pits do not play any role for the force between the bodies, but high asperities are very important because they can approach close to the opposite body and even get into contact with it. The deviation of roughness from the normal distribution was already stressed previously [54]. It was demonstrated [39,40] that for gold films the high peaks are well described by the extreme value statistics, but the conclusion was made from

the analysis of much rougher films. The case demonstrated in Figure 3 corresponds to a smoother film, but the high peak tail is also well described by the extreme value statistics as the solid blue curve shows.

In general case this statistics is described by the cumulative distribution $\mathcal{P}(z)$ in the form [62]

$$\mathcal{P}(z) = 1 - \exp\left[-\exp\left(\frac{z-\mu}{\beta}\right)\right], \tag{14}$$

where μ and β are the parameters. A characteristic feature of this distribution is given by the relation

$$\ln[-\ln(1-\mathcal{P}(z))] = A + Bz. \tag{15}$$

The parameters A and B used in [39,40] are obviously related to μ and β. The corresponding probability density has the following form

$$f(z) = B\Phi\exp(-\Phi), \quad \ln\Phi = A + Bz. \tag{16}$$

In our case the values of these parameters are $A = 0.7528$ and $B = 0.1179$ nm^{-1}. This distribution is shown in Figure 3 by the blue solid line. It describes well the AFM data for the heights $z > 3w$.

For what follows we need a relation between the pressure applied to the bodies in contact and the average distance between them. It is defined by the roughness and plasticity limit of the substrate material. The rough substrate is modeled as an ensemble of columns with a random height and fixed cross-section l_a^2, which is defined by the correlation length l_a. The highest asperities get into contact with a flat stiff surface of the cantilever. Only a few asperities are in contact and pressure on them exceeds the plasticity limit P_f. These columns are deformed plastically reducing their height to a uniform value equal to h_0 that is the average distance between the bodies at contact. As the result the pressure on the asperities, which are in contact with the cantilever, is equal to P_f.

If the surfaces are pressed together with the force F, this force is balanced by the deformed columns and the balance can be expressed as $F = \sum_i P_f l_a^2$, where the sum is taken on the columns, which are higher than h_0. This sum can be expressed via the probability density function $f(z)$ as

$$F = P_f S \int_{h_0}^{\infty} dz f(z), \tag{17}$$

where S is the nominal area of contact. Since the average distance between the bodies in contact h_0 is larger than $3w$, we can use the asymptotic distribution (16). Dividing (17) by S one finds the relation between the applied pressure P and the average distance h_0:

$$P = P_f e^{-\Phi(h_0)}. \tag{18}$$

This relation will be used in Section 4.4 to estimate the coefficient of compliance.

3.3. Total Force

As input data in Equation (7) we used $\varepsilon(\omega)$ for Si taken from the handbook [63], which is well documented, and the corresponding function for Au [55] that was measured in a wide range of frequencies. The conductivity of silicon was neglected since it is not important for the distances of interest. On the other hand, the Drude parameters for gold were taken to be $\omega_p = 7.84$ eV and $\gamma = 49$ meV as extrapolated in [55], but their exact values are not crucially important in the short distance range, because the far- and mid-infrared frequencies do not give large contribution to the force at $h < 30$ nm.

In actual calculation of the roughness contribution with Equation (10), we used the experimental function $f(z)$ while $z < 5w$ but for larger heights the relation (16) was used. The result is shown in Figure 4 for a few values of the average distance between the bodies at contact. One can see that the roughness contribution becomes very significant and

even dominates when the bodies approach the contact. It occurs because high asperities approach very close to the opposite body and the number of such asperities is much larger than that predicted by the normal distribution. When the bodies are separated further apart the roughness contribution decreases quickly and asymptotically behaves with the distance as $\sim P_L(h)w^2/h^2$ that coincides with the prediction of the perturbation theory.

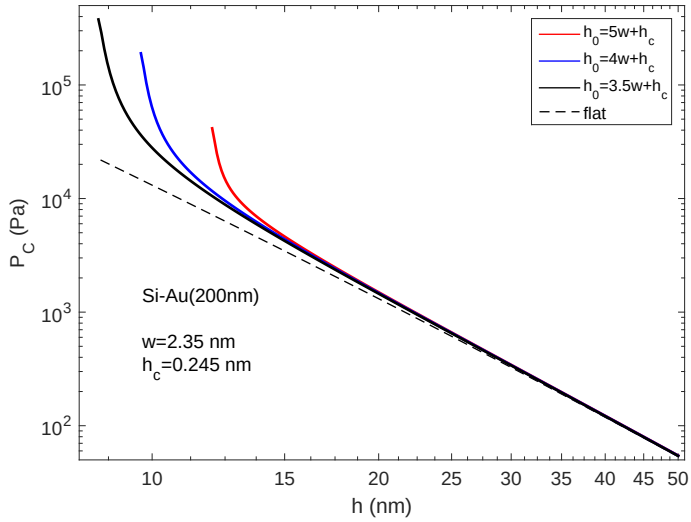


Figure 4. The Casimir force (CF) between Si (smooth) and Au (rough) plates as a function of distance. The force is shown for three average distances at contact $h_0 = 8.46,\ 9.66,\ 12.02$ nm. The dashed line corresponds to the force between two flat plates.

At short separations the highest asperities get into contact with the flat plate and deform plastically. In the area of real contact the modified Lifshitz force (11) becomes important. If no external load, the equilibrium distance in the area of real contact is $h_{eq} = h_c$ and according to Equation (11) the contact force is equal to zero. However, for nonzero adhesion energy Γ the equilibrium distance at contact h_{eq} does not coincide with h_c and the contact force $P_{cont}(h)$ becomes finite. Although the area of real contact is not large, the forces acting in this area are significant. As a result the contact contribution at some conditions can even dominate in the total force. It depends on the details of the roughness distribution, on the repulsive component of the force, and on the value of plastic flow stress of the deformable materials. As we already indicated, $P_{cont}(h)$ is outside of the scope of this paper. Here we concentrated on the effects of nonideality. One of such effects is the deviation of the total force from the Lifshitz contribution. For this purpose the deviation due to roughness is sufficient to understand the tendency.

4. Contribution of Roughness and the Background Effects to the Shape of the Cantilever

In this section we investigate influence of different effects on the shape of the cantilever. One can distinguish the effect related to the external force acting on the cantilever from the effects related to the internal properties of the cantilever. The shape of the cantilever is described by the theory of elasticity resulting in different equations for these two kinds of effects.

The cantilevers are fabricated using silicon on insulator (SOI) wafers [41] where the top layer is 10 μm thick single crystal silicon separated by a 1 μm SiO_2 layer from the base Si substrate (350 μm thick). The fabrication procedure includes patterning and etching of the cantilevers in the top layer and their release by etching away the base layer from the back side. It is a multistep process, which inevitably leaves a residual stress in the cantilevers. The technology is tuned to minimise this stress but it is not possible to exclude it

completely. The residual stress manifests itself as an initial curvature of the free (unadhered) cantilever. This curvature can be measured before assembling the cantilevers with the counter substrate, to which the free ends adhere.

Besides that the providers of SOI wafers guarantee that the thickness of the top layer is homogeneous within 5–10%. This means that the thickness of cantilevers t can vary slowly along its length and the variation can be as large as 1 μm. This variation can be measured using, for example, an infrared interferometer, for which Si cantilevers are transparent and the interference contrast is formed due to reflection from both sides. In addition, the rough substrate is not completely stiff. It has a finite compliance because high asperities can be deformed. It makes the adhered end of the cantilever not firmly fixed. All these effects will change the classic (without external force) shape that will be slightly different from that described by Equation (2). This difference has to be taken into account to extract the force from the raw data and for that we have to modify the equation used in [42].

4.1. Generalised Equation for the Shape of the Cantilever

Consider bending of a rectangular elastic beam with the total length L, for which the left end is firmly fixed at the height H and the right end is adhered to the substrate as shown in Figure 5. In the macroscopic description the rough surface of the substrate is considered as a deformable smooth surface, for which the undeformed state coincides with the level $h = h_0$ as shown explicitly in Figure 1. If the origin of x-coordinate is chosen at the right end, then the cantilever is detached from the substrate at $x_s = L - s$ and the left end is at the position $x = L$. Since the substrate has a finite compliance the beam can penetrate into the substrate in the adhered area to the depth $\delta(x)$. The unadhered part of the beam in the interval $x_s < x < L$ is separated from the substrate by a gap $v(x) = h(x) - h_0$. If $u(x)$ is the bending of the cantilever midline as shown in Figure 5, then there is a simple geometrical relation between $v(x)$ and $u(x)$ in the entire domain $0 < x < L$ that is

$$v(x) = H + t(L)/2 - t(x)/2 - u(x) + \delta(x). \tag{19}$$

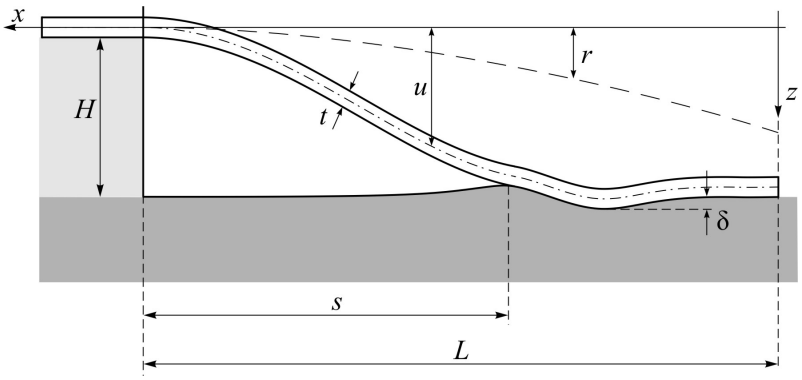


Figure 5. Adhered cantilever in the most general case. The cantilever has a nonhomogeneous thickness $t(x)$ and has a nonzero initial bending $r(x)$ shown by the thick dashed line. The rough substrate is modelled as a deformable smooth surface and the penetration of the adhered part of the cantilever into the substrate is $\delta(x)$. The function $u(x)$ describes the bending of the midline of the adhered cantilever.

Using the theory of beam bending [64] one can deduce the following differential equation that describes the shape of adhered cantilever:

$$\left[D(x)\tilde{u}''(x)\right]'' = \beta(x), \quad \tilde{u}(x) = u(x) - r(x), \tag{20}$$

where prime means the derivative on x, $r(x)$ is the initial shape of the cantilever before the adhesion, $D(x) = Et^3(x)/12$ is the running flexural rigidity of the beam, and $\beta(x)$ is the bending stress. To describe the effective deformation of the substrate we use the Winkler

model [45,46,65] that postulates a linear dependence of the penetration δ on the normal stress at the substrate surface $\sigma_z = \beta$ so that

$$\delta(x) = -A_W \beta(x), \tag{21}$$

where $A_W > 0$ is the compliance coefficient, which is defined by the deformation properties of the rough substrate that follows from Equation (18).

The stress $\beta(x)$ that enters Equations (20) and (21) is due to the mechanical reaction of the substrate in the adhered area or due to the external (Casimir) forces acting on the unadhered part of the beam. In the latter case it is

$$\beta(x) = P_C(h(x)) = P_C(v(x) + h_0). \tag{22}$$

Taking into account that $v(x) = 0$ in the adhered area and using the Derjaguin self-consistent approach [47] for the unadhered part one can use Equations (19)–(22) to deduce the equation that describes bending of the midline of the cantilever $u(x)$. The result can be written in the form

$$\left[D(x)u''(x)\right]'' = \beta_r(x) + \begin{cases} \beta_1(u(x) + t(x)/2), & 0 < x < x_s, \text{ (adhered)} \\ \beta_2(u(x) + t(x)/2), & x_s < x < L, \text{ (unadhered)} \end{cases} \tag{23}$$

where $\beta_r(x)$ is defined as $\beta_r(x) = [D(x)r''(x)]''$, the function $\beta_1(X)$ has an explicit expression $\beta_1(X) = (H + t(L)/2 - X)/A_W$, while the function $\beta_2(X)$ is defined implicitly as a solution of the equation $\beta_2(X) = P_C(H + t(L)/2 + h_0 - X - A_W\beta_2(X))$.

The differential Equation (23) has to be solved with the following boundary conditions

$$u''(0) = 0, \quad u'''(0) = 0, \quad u(L) = 0, \quad u'(L) = -t'(L)/2. \tag{24}$$

Here the first two conditions correspond to the absence of bending moment and shearing force at the right end. The other two conditions describe the firmly fixed left end of the cantilever. The last condition follows from the fact that the bottom line of the cantilever has zero derivative at $x = L$. The boundary problem (23), (24) can be solved, for example, by shooting method using the Runge–Kutta procedure. Let us consider now a few relevant special cases.

4.2. Influence of Roughness

If the external force P_C is acting on an ideally homogeneous cantilever $t(x) = t_0$ that has no initial bending $r(x) = 0$ and the substrate is stiff $A_W = 0$, then the adhered end is completely immobilised. In this case it is convenient to shift the origin of the coordinate system to the point $x = x_s$, where the cantilever is detached from the substrate, and the left end will be at $x = s$. The flexural rigidity D is now a constant and Equation (23) gets the form [42]

$$\begin{aligned} D\frac{d^4u}{dx^4} &= P_C(H + h_0 - u(x)), \quad 0 < x < s, \\ u(0) = H, \quad u'(0) &= 0, \quad u(s) = u'(s) = 0. \end{aligned} \tag{25}$$

The boundary conditions for this problem means that both ends of the cantilever are firmly fixed at $x = 0$ and $x = s$.

It has to be stressed that experimentally we measure the shape of the cantilever along its top surface but not along the midline. The observed shape $u_t(x)$ is related to $u(x)$ by a simple geometric relation $u_t(x) = u(x) + t(s)/2 - t(x)/2$. Therefore, for the case $t(x) = t_0$ the function $u(x)$ gives the complete information on the experimentally observed shape.

If $P_C = 0$ the Equation (25) becomes linear and has a simple solution (2). When the right hand side in (25) is given by the force between flat surfaces $P_C(h) = P_L(h)$, then the equation is nonlinear because $h(x) = H + h_0 - u(x)$ depends on u and the equation has to

be solved numerically. For $P_L(h)$ approximated by Equation (4), the solution is shown in Figure 2.

In more general case, when the force as a function of the separation is taken from the data presented in Figure 4, the deviation from the classic shape is shown in Figure 6. The solid lines demonstrate the results for the total force that includes both the Lifshitz and roughness contributions. Each curve corresponds to the critical parameter $K = K_c$, where K is defined as in (5) with $P_0 = P_L(h_0)$ taken as the force between flat surfaces. For three values $h_0 = 8.49,\ 9.66,\ 12.02$ nm the critical parameters are $K_c^{rough} = 11.76,\ 11.96,\ 12.47$, respectively, and the corresponding P_0 are $P_0 = (2.23,\ 1.47,\ 0.72) \times 10^4$ Pa. The values of K are presented for $E = 160$ GPa (silicon) and $H = t = 10$ μm. The thin dashed curve demonstrates the deviation from $u_0(x)$ for flat surfaces separated by the distance $h_0 = 9.66$ nm. It corresponds to the critical values for flat surfaces $K_c^{flat} = 14.56$. The dash-dotted curve shows the deviation for flat surfaces that corresponds to $K^{flat} = 11.96$ that is smaller than the critical value K_c^{flat}.

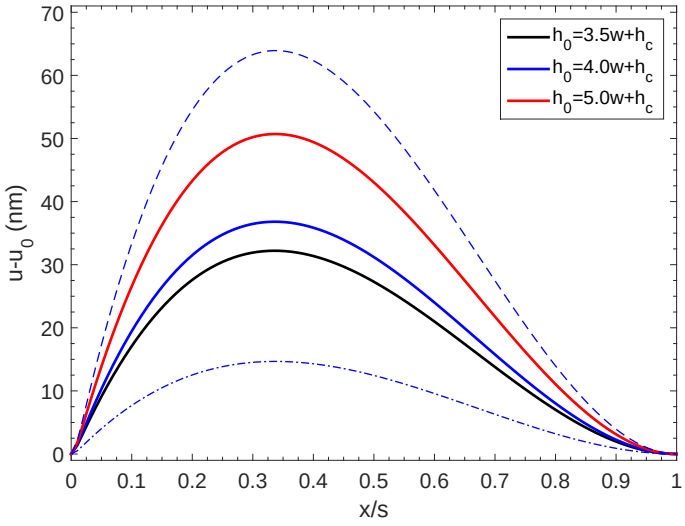


Figure 6. Deviation from the classic shape for the forces shown in Figure 4 (solid lines). The results are presented for $H = t = 10$ μm and the parameter K is close to the critical value K_c for each curve. The point $x/s = 0$ corresponds to the point of attachment to the substrate and $x/s = 1$ to the right side of the support. The colours are related to the value h_0, which are the same as in Figure 4. The thin dashed line corresponds to the critical situation ($K_c^{flat} = 14.56$) between flat surfaces for $h_0 = 9.66$ nm. The thin dash-dotted curve shows the deviation between flat surfaces corresponding to the same h_0 but for $K = 11.96$, which is realised for the same s as for the rough surfaces.

Intuitively one would expect that the deviation $u - u_0$ will be larger when the force increases. However, it is true if we compare the deviations corresponding to the same unadhered length $s = K(Et^3H/12P_0)^{1/4}$. The solid and dash-dotted blue curves correspond to the same length $s = 3.69$ mm and indeed the deviation for rough surfaces is larger than that for flat surfaces. On the other hand, the critical situation for flat surfaces is realised for longer unadhered length $s = 4.49$ mm and the deviation can be larger than that for the rough surfaces (dashed curve). Such long s cannot be realised for rough surfaces because the force is too strong. We can conclude that in spite of a significant increase in the force between rough surfaces the deviation from the classic shape, which can be measured in the experiment, decreases because the larger force corresponds to the shorter unadhered length. Nevertheless, the deviation is still well in the measurable range.

4.3. Stiff Substrate

In this section we consider a stiff substrate $A_W = 0$ but the cantilever can be bent initially $r(x) \neq 0$ and its thickness can be inhomogeneous $t = t(x)$. The main interest is how the classic shape of the cantilever $u_0(x)$ changes due to nonideality of the cantilever. It is expected that these effects are small in comparison with the classic shape (2) or equivalently that maximum deviation from (2) is much less than the height H. Since the CF gives also only a small correction to the classic shape, it is reasonable to assume that the effects of nonideality do not depend on the force and in the first approximation we can put $P_C(h) = 0$. For a stiff substrate without external forces the equation describing the shape becomes linear:

$$\left[D(x)\tilde{u}''(x)\right]'' = 0, \quad \tilde{u}(x) = u(x) - r(x). \tag{26}$$

As in Section 4.2 it is convenient to choose the origin of the x-coordinate in the point where the cantilever is detached from the substrate, then the equation is defined in the domain $0 < x < s$ and the boundary conditions are

$$u(0) = H + t(s)/2 - t(0)/2, \quad u'(0) = -t'(0)/2, \quad u(s) = 0, \quad u'(s) = -t'(s)/2. \tag{27}$$

Because Equation (26) is linear the effects of the initial curvature and inhomogeneous thickness can be considered separately. Moreover, the equation can be solved analytically. First, let us consider the case of finite curvature of the cantilever with a homogeneous thickness $t(x) = t_0$, $t'(x) = 0$. Since the cantilever is firmly fixed at $x = s$, the function $r(x)$ obeys the conditions $r(s) = r'(s) = 0$. The solution of Equation (26) can be presented as

$$\begin{aligned} u(x) = \left[2H - 2r(0) - sr'(0)\right](x/s)^3 + \left[-3H + 3r(0) + 2sr'(0)\right](x/s)^2 + \\ H + r(x) - r(0) - r'(0)x, \end{aligned} \tag{28}$$

In real experiment the cantilever is slightly curved and can be described as a piece of a circle with a large radius $\mathcal{R}$. Then the function $r(x)$ is

$$r(x) = \frac{s^2}{2\Delta H}\left[1 - \sqrt{1 - \frac{4\Delta H^2}{s^2}(1 - x/s)^2}\right], \quad \mathcal{R} \approx \frac{s^2}{2\Delta H}. \tag{29}$$

Here instead of the curvature radius $\mathcal{R}$ we introduced more practical parameter $\Delta H = r(0) - r(s)$ that is the sag (positive or negative) of the cantilever. The fabrication technology is tuned to minimise the sag that is $\Delta H \sim 1$ μm. Since the unadhered length is s = 3–5 mm the parameter $2\Delta H/s \sim 10^{-3}$ is small. The first nonvanishing term in the expansion of (29) gives the parabolic behaviour $r(x) = \Delta H(1 - x/s)^2$. If we put this function into the solution (28), all the terms containing ΔH will cancel. It means that the initial bending of the cantilever does not contribute to the shape of the adhered cantilever. This could be expected because, while $r(x)$ is described by a polynomial of less than the fourth order in x and the boundary conditions do not depend on r, the solution of the fourth-order differential equation cannot be sensitive to $r(x)$. The second term in the expansion of (29) will change the classic shape of the adhered cantilever slightly. Its effect will be of the order of $\Delta H(\Delta H/s)^2 \sim 10^{-3}$ nm that is negligible. Thus, we can conclude that in realistic situations the initial curvature of the cantilever can be neglected.

In contrast with the finite curvature, the inhomogeneous thickness of the cantilever has an observable effect. As was explained above, the top layer of SOI wafer with a diameter of 100 mm can vary 5–10%. On the length $s = 5$ mm one can expect 1% linear variation of the thickness. Let the total thickness variation be $\Delta t = t(s) - t(0)$, then $t(x)$ can be presented as

$$t(x) = t(0)(1 + \alpha x/s), \quad \alpha = \frac{\Delta t}{t(0)} \lesssim 0.01, \tag{30}$$

where α is a small positive or negative parameter. Equation (26) is now modified to the following

$$\left[(1+\alpha x/s)^3 u''(x)\right]'' = 0, \quad 0 < x < s, \tag{31}$$

Since $t(x)$ is a linear function of x, the same equation describes the top $u_t(x)$ and bottom $u_b(x)$ surfaces of the cantilever. The boundary conditions are formulated directly for the bottom surface and have for $u_b(x)$ the simplest form that is

$$u_b(0) = H, \quad u_b'(0) = 0, \quad u_b(s) = 0, \quad u_b'(s) = 0. \tag{32}$$

Since α is small we can look for the solution as a series in α. The first nonvanishing term is

$$\begin{aligned} \delta u_b(x) = u_b(x) - u_{0b}(x) = -3\alpha H\xi^2(1-\xi)^2, \\ u_{0b}(x) = H(1-3\xi^2+2\xi^3), \quad \xi = x/s. \end{aligned} \tag{33}$$

One can see that the sign of the correction is defined by the sign of α. The external force always gives a positive correction to (u_{0b}), but the correction due to inhomogeneous thickness is negative if at the adhered end it is thinner and positive in the opposite case. For the parameters expected in the experiment $H = t(0) = 10$ μm the result is shown in Figure 7. As we already mentioned, the directly observed shape is $u_t(x) = u_b(x) - t(x) + t(s)$.

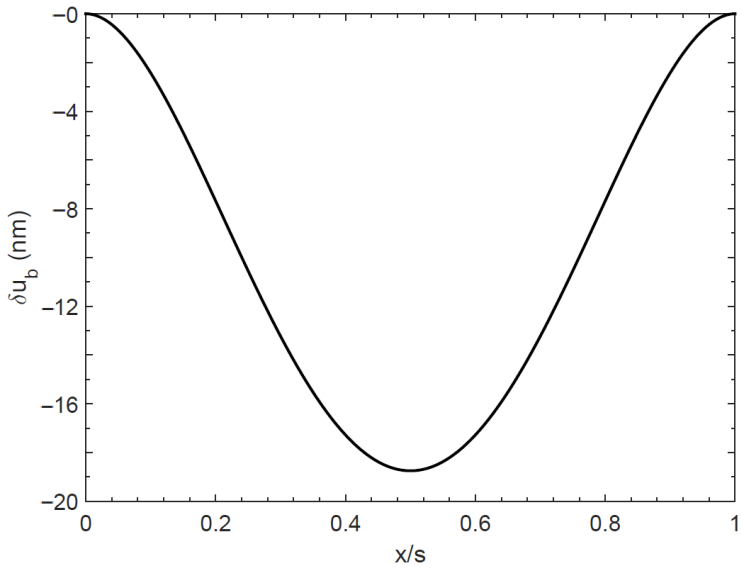


Figure 7. Deviation from the classic shape $u_{0b}(x)$ (see Equation (33)) due to linear variation of the thickness $t(x) = t(0)(1+\alpha x/s)$. The result is presented for $\alpha = 0.01$ and $H = 10$ μm.

Maximum variation of the thickness along the unadhered part of the cantilever is expected as 1%. One can see that this variation gives a measurable change in the classic shape, which is comparable with the effect of the CF as shown in Figure 6 for the same parameters H and $t(0)$. The second order correction $\sim \alpha^2$ to the classic shape can be neglected since it is on the level of the experimental errors. We can conclude that the variation of thickness is an important background effect that has to be carefully excluded from the experimental data. For that it is important to measure the function $t(x)$ experimentally.

4.4. Finite Compliance of the Substrate

Consider now the case when $r(x) = 0$, $t(x) = t_0$ but the compliance of the substrate A_W is nonzero. Our interest here is the modification of the classic shape due to finite compliance. In Equation (23) we can exclude the external force $P_C(h(x))$, exclude the term

$\beta_r(x) = 0$ related to the initial curvature, and take $D(x) = D = Et_0^3/12$ as a constant. In this case the equation can be solved analytically, but to present it in a readable form it is convenient to put the origin of x-coordinate at the very end of the adhered part of the cantilever as shown in Figure 5. The equation describing the shape of the cantilever is

$$D\frac{\mathrm{d}^4u}{\mathrm{d}x^4} = \begin{cases} (H-u)/A_W, & 0 < x < L-s, \text{ (adhered)} \\ 0, & L-s < x < L \text{ (unadhered)} \end{cases} \tag{34}$$

that has to be solved with the boundary conditions

$$u''(0) = 0, \quad u'''(0) = 0, \quad u(L) = 0, \quad u'(L) = 0. \tag{35}$$

In the adhered domain the equation is

$$\frac{\mathrm{d}^4u}{\mathrm{d}x^4} = \frac{4k^4}{L^4}(H-u), \quad 0 < x < L-s;$$
$$u''(0) = u'''(0) = 0; \quad k = \left(\frac{3L^4}{Et_0^3A_W}\right)^{1/4}. \tag{36}$$

Normalising x-coordinate with the total length L but keeping the same notation for the normalised coordinate $\xi = x/L$, one can present the solution in the following form

$$u(x) = H + e^{k\xi}(A_1\cos k\xi + A_2\sin k\xi) + e^{-k\xi}[(A_1 - 2A_2)\cos k\xi + A_2\sin k\xi], \quad \xi = x/L, \tag{37}$$

where $A_{1,2}$ are arbitrary constants. On the other hand, in the domain $L-s < x < L$ the function is described by the equation

$$\frac{\mathrm{d}^4u}{\mathrm{d}x^4} = 0, \quad L-s < x < L;$$
$$u(L) = u'(L) = 0 \tag{38}$$

and the solution is

$$u(x) = B_1\xi^3 + B_2\xi^2 - (3B_1 + 2B_2)\xi + 2B_1 + B_2, \tag{39}$$

where $B_{1,2}$ are also arbitrary constants. Four unknown constants $A_{1,2}$ and $B_{1,2}$ are determined by matching the functions (37) and (39) and their three derivatives in the point $x = L - s$. In principle, this procedure can be performed analytically but the result is cumbersome and we do the matching numerically.

Before presenting the final result it is important to know the expected value of the compliance parameter A_W. It is defined by the roughness and by the plasticity limit of the substrate material and can be found from the relation (18) between the applied pressure and average distance between the bodies. To compare this relation to the Winkler model (21) we can linearize Equation (18) near h_0 and find for the compliance coefficient as

$$A_W = \frac{e^{\Phi(h_0)}}{B\Phi(h_0)P_f}. \tag{40}$$

The plasticity limit for gold is $P_f = 0.205$ GPa but for nanosized samples it can be somewhat larger [56,66]. For $h_0 = nw + h_c$ used to calculate the force in Figure 4, where $n = 3.5,\ 4\ ,5$ we find $A_W = (2.29,\ 4.68,\ 29.4) \times 10^3$ nm/GPa. Knowing A_W one can find the parameter k that enters in the shape of the cantilever in the adhered domain (37); it gives $k = 267,\ 224,\ 141$ for $L = 5$ mm. Resolving the matching condition with respect to the constants $A_{1,2}$ and $B_{1,2}$, we find the solution $u(x)$ in the entire domain $0 < x < L$. The result is shown in Figure 8.

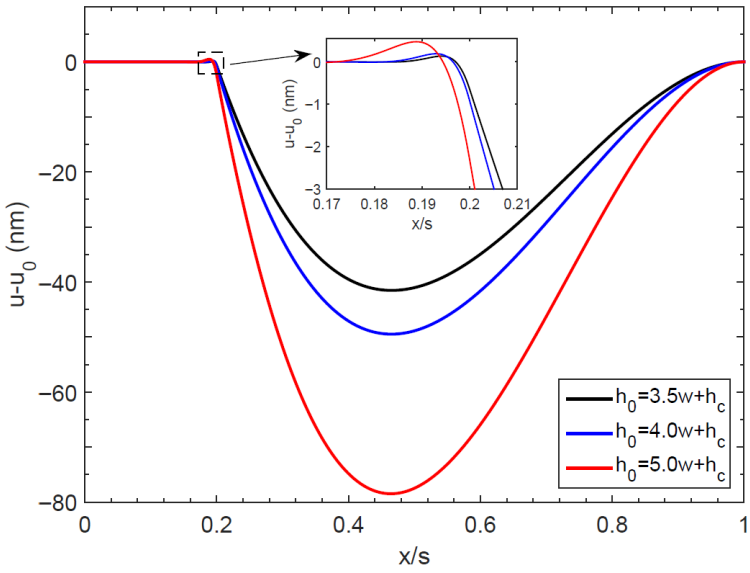


Figure 8. Deviation from the classic shape (2) due to finite compliance of the rough substrate for $L = 5$ mm and $s = 4$ mm. The values of h_0 are the same as in Figure 4. The results are presented for three values of average distance between the bodies at contact. The inset demonstrates the detailed behaviour near the transition from the adhered to unadhered state.

As one can see, the effect of finite compliance is even more important than the variation of the thickness $t(x)$. The transition region from adhered to unadhered part of the cantilever is about 40 μm, while for the CF the width of the transition region is estimated as 300 μm. Effectively it looks like a kink at the adhered end, although the inset in Figure 8 demonstrates that the transition is smooth. The inset shows also that the cantilever penetrates into the substrate but the penetration depth is rather small.

5. Conclusions

Experimental measurement of the Casimir forces at distances shorter than 30 nm is problematic due to pull-in instability and due to roughness effect. A method of adhered cantilever proposed recently [41] allows for the overcoming of the instability problem and proposes an approach to treat the roughness effect. In this paper we addressed the way to calculate the roughness contribution to the force beyond the perturbation theory. In comparison with the previous analysis [39,40] we demonstrated that the roughness contribution is especially important for the surfaces with a relatively small rms roughness. When the bodies approach the contact the roughness contribution starts to grow so strongly that it dominates the total force and can be one order of magnitude larger than the force between flat surfaces separated by the same distance. It is manifested as a strong deviation from the power law behaviour at short separations. In contrast with [39,40], we also took into account the repulsive contribution when the bodies get into contact. It allowed calculation of the force even in the case when the bodies are in direct contact. Without this repulsive contribution the force would diverge at contact. Our calculations are justified up to the point of direct contact but still restricted by the limit of small load. When the load is not negligible there is an additional contact contribution to the force that has to be analysed with different method and will be presented elsewhere.

In any experiment measuring the forces there are a number of background effects, which are sometimes larger than the measured force. For example, the main background effect for the Casimir forces at $h > 30$ nm measured with the elastic suspension method is the residual electrostatic force [9–13]. At shorter separations the electrostatic forces are not so critical, but the elastic suspension cannot be used due to the pull-in instability. The adhered cantilever method gives the opportunity to measure the forces at small

distances but there are some background effects that have to be excluded from the data. These effects have been discussed in Section 4.

In the method of adhered cantilever the force is measured as the deviation of the shape of the cantilever from a known classic shape. Here we indicated three potentially important effects, which are able to change slightly the classic shape even if there is no force acting on the cantilever. Technologically it is not possible to fabricate cantilevers without residual stress. This stress results in a small initial bending of the cantilever. We demonstrated that, while the initial bending is parabolic, it does not influence the shape of the adhered cantilever. Deviation from the parabolic bending is too small to provide a measurable effect in the adhered state. Thus, a small initial bending of the cantilever does not influence the shape of the adhered cantilever on a measurable level.

Fabrication technology of the cantilevers cannot guarantee completely homogeneous thickness of the cantilevers. The variation of the thickness up to one percent is expected. This variation can influence the shape of the adhered cantilever. It was shown that inhomogeneous thickness can contribute to the classic shape on the same level as the expected Casimir force. To control this effect it is necessary to measure thickness of the cantilever along its length. If this variation is known, one can reliably predict its effect on the shape of the adhered cantilever.

We also estimated the effect of finite compliance of the rough substrate on the classic shape of the cantilever. The calculations have been performed within the linear Winkler model but the compliance coefficient was estimated using a realistic roughness statistics of the substrate. The result showed that the effect of finite compliance is also important and has to be carefully excluded from the raw data. Influence of finite compliance depends significantly on the average distance between the bodies at contact.

Author Contributions: Conceptualisation, I.A.S. and V.B.S.; software, A.A.Y.; validation, I.A.S., A.A.Y. and V.B.S.; writing—original draft preparation, V.B.S.; writing—review and editing, I.A.S. and A.A.Y.; funding acquisition, V.B.S. All authors have read and agreed to the published version of the manuscript.

Funding: This research was funded by the Russian Science Foundation grant number 20-19-00214.

Institutional Review Board Statement: Not applicable.

Informed Consent Statement: Not applicable.

Data Availability Statement: Data are available on request from V.B.S. (svetovoy@yandex.ru).

Acknowledgments: Authors are grateful to George Palasantzas for providing the AFM data for Au sample.

Conflicts of Interest: The authors declare no conflict of interest.

Abbreviations

The following abbreviations are used in this manuscript:

vdW	van der Waals
CF	Casimir forces
MEMS/NEMS	Micro/Nanoelectromechanical systems
AFM	Atomic Force Microscope
rms	root-mean-square
SOI	silicon on insulator

References

1. London, F. Zur Theorie und Systematik der Molekularkräfte. *Z. Phys.* **1930**, *63*, 245. [CrossRef]
2. Casimir, H.B.G.; Polder, D. The Influence of Retardation on the London-van der Waals Forces. *Phys. Rev.* **1948**, *73*, 360–372. [CrossRef]
3. Casimir, H.B.G. On the Attraction between Two Perfectly Conducting Plates. *Proc. Kon. Ned. Akad. Wet.* **1948**, *51*, 793.
4. Lifshitz, E.M. The theory of molecular attractive forces between solids. *Sov. Phys. JETP* **1956**, *2*, 73.

5. Dzyaloshinskii, I.E.; Lifshitz, E.M.; Pitaevskii, L.P. General theory of van der Waals' forces. *Sov. Phys. Uspekhi* **1961**, *4*, 153–176. [CrossRef]
6. Klimchitskaya, G.L.; Mohideen, U.; Mostepanenko, V.M. The Casimir force between real materials: Experiment and theory. *Rev. Mod. Phys.* **2009**, *81*, 1827–1885. [CrossRef]
7. Rodriguez, A.W.; Capasso, F.; Johnson, S.G. The Casimir effect in microstructured geometries. *Nat. Photonics* **2011**, *3*, 211–221. [CrossRef]
8. Woods, L.M.; Dalvit, D.A.R.; Tkatchenko, A.; Rodriguez-Lopez, P.; Rodriguez, A.W.; Podgornik, R. Materials perspective on Casimir and van der Waals interactions. *Rev. Mod. Phys.* **2016**, *88*, 045003. [CrossRef]
9. Lamoreaux, S.K. Demonstration of the Casimir Force in the 0.6 to 6 μm Range. *Phys. Rev. Lett.* **1997**, *78*, 5–8. [CrossRef]
10. Harris, B.W.; Chen, F.; Mohideen, U. Precision measurement of the Casimir force using gold surfaces. *Phys. Rev. A* **2000**, *62*, 052109. [CrossRef]
11. Chan, H.B.; Aksyuk, V.A.; Kleiman, R.N.; Bishop, D.J.; Capasso, F. Quantum Mechanical Actuation of Microelectromechanical Systems by the Casimir Force. *Science* **2001**, *291*, 1941–1944. [CrossRef]
12. Bressi, G.; Carugno, G.; Onofrio, R.; Ruoso, G. Measurement of the Casimir Force between Parallel Metallic Surfaces. *Phys. Rev. Lett.* **2002**, *88*, 041804. [CrossRef]
13. Decca, R.S.; López, D.; Fischbach, E.; Krause, D.E. Measurement of the Casimir Force between Dissimilar Metals. *Phys. Rev. Lett.* **2003**, *91*, 050402. [CrossRef]
14. Decca, R.; López, D.; Fischbach, E.; Klimchitskaya, G.; Krause, D.; Mostepanenko, V. Precise comparison of theory and new experiment for the Casimir force leads to stronger constraints on thermal quantum effects and long-range interactions. *Ann. Phys.* **2005**, *318*, 37–80. [CrossRef]
15. Sushkov, A.O.; Kim, W.J.; Dalvit, D.A.R.; Lamoreaux, S.K. Observation of the thermal Casimir force. *Nat. Phys.* **2011**, *7*, 230–233. [CrossRef]
16. Chang, C.C.; Banishev, A.A.; Castillo-Garza, R.; Klimchitskaya, G.L.; Mostepanenko, V.M.; Mohideen, U. Gradient of the Casimir force between Au surfaces of a sphere and a plate measured using an atomic force microscope in a frequency-shift technique. *Phys. Rev. B* **2012**, *85*, 165443. [CrossRef]
17. Bimonte, G.; López, D.; Decca, R.S. Isoelectronic determination of the thermal Casimir force. *Phys. Rev. B* **2016**, *93*, 184434. [CrossRef]
18. Liu, M.; Xu, J.; Klimchitskaya, G.L.; Mostepanenko, V.M.; Mohideen, U. Precision measurements of the gradient of the Casimir force between ultraclean metallic surfaces at larger separations. *Phys. Rev. A* **2019**, *100*, 052511. [CrossRef]
19. Buks, E.; Roukes, M.L. Stiction, adhesion energy, and the Casimir effect in micromechanical systems. *Phys. Rev. B* **2001**, *63*, 033402. [CrossRef]
20. Capasso, F.; Munday, J.N.; Iannuzzi, D.; Chan, H.B. Casimir Forces and Quantum Electrodynamical Torques: Physics and Nanomechanics. *IEEE J. Sel. Top. Quant.* **2007**, *13*, 400–414. [CrossRef]
21. Esquivel-Sirvent, R.; Reyes, L.; Bárcenas, J. Stability and the proximity theorem in Casimir actuated nano devices. *New J. Phys.* **2006**, *8*, 241. [CrossRef]
22. Esquivel-Sirvent, R.; Palomino-Ovando, M.A.; Cocoletzi, G.H. Pull-in control due to Casimir forces using external magnetic fields. *Appl. Phys. Lett.* **2009**, *95*, 051909. [CrossRef]
23. Broer, W.; Palasantzas, G.; Knoester, J.; Svetovoy, V.B. Significance of the Casimir force and surface roughness for actuation dynamics of MEMS. *Phys. Rev. B* **2013**, *87*, 125413. [CrossRef]
24. Broer, W.; Waalkens, H.; Svetovoy, V.B.; Knoester, J.; Palasantzas, G. Nonlinear Actuation Dynamics of Driven Casimir Oscillators with Rough Surfaces. *Phys. Rev. Appl.* **2015**, *4*, 054016. [CrossRef]
25. Palasantzas, G.; Sedighi, M.; Svetovoy, V.B. Applications of Casimir forces: Nanoscale actuation and adhesion. *Appl. Phys. Lett.* **2020**, *117*, 120501. [CrossRef]
26. Smullin, S.J.; Geraci, A.A.; Weld, D.M.; Chiaverini, J.; Holmes, S.; Kapitulnik, A. Constraints on Yukawa-type deviations from Newtonian gravity at 20 microns. *Phys. Rev. D* **2005**, *72*, 122001. [CrossRef]
27. Kapner, D.J.; Cook, T.S.; Adelberger, E.G.; Gundlach, J.H.; Heckel, B.R.; Hoyle, C.D.; Swanson, H.E. Tests of the Gravitational Inverse-Square Law below the Dark-Energy Length Scale. *Phys. Rev. Lett.* **2007**, *98*, 021101. [CrossRef]
28. Decca, R.S.; López, D.; Fischbach, E.; Klimchitskaya, G.L.; Krause, D.E.; Mostepanenko, V.M. Tests of new physics from precise measurements of the Casimir pressure between two gold-coated plates. *Phys. Rev. D* **2007**, *75*, 077101. [CrossRef]
29. Sushkov, A.O.; Kim, W.J.; Dalvit, D.A.R.; Lamoreaux, S.K. New Experimental Limits on Non-Newtonian Forces in the Micrometer Range. *Phys. Rev. Lett.* **2011**, *107*, 171101. [CrossRef]
30. Chen, Y.J.; Tham, W.K.; Krause, D.E.; López, D.; Fischbach, E.; Decca, R.S. Stronger Limits on Hypothetical Yukawa Interactions in the 30–8000 nm Range. *Phys. Rev. Lett.* **2016**, *116*, 221102. [CrossRef]
31. Mostepanenko, V.M.; Klimchitskaya, G.L. The State of the Art in Constraining Axion-to-Nucleon Coupling and Non-Newtonian Gravity from Laboratory Experiments. *Universe* **2020**, *6*, 147. [CrossRef]
32. Nesvizhevsky, V.V.; Pignol, G.; Protasov, K.V. Neutron scattering and extra-short-range interactions. *Phys. Rev. D* **2008**, *77*, 034020. [CrossRef]
33. Kamiya, Y.; Itagaki, K.; Tani, M.; Kim, G.N.; Komamiya, S. Constraints on New Gravitylike Forces in the Nanometer Range. *Phys. Rev. Lett.* **2015**, *114*, 161101. [CrossRef]

34. Haddock, C.C.; Oi, N.; Hirota, K.; Ino, T.; Kitaguchi, M.; Matsumoto, S.; Mishima, K.; Shima, T.; Shimizu, H.M.; Snow, W.M.; et al. Search for deviations from the inverse square law of gravity at nm range using a pulsed neutron beam. *Phys. Rev. D* **2018**, *97*, 062002. [CrossRef]
35. Van Zwol, P.J.; Palasantzas, G.; van de Schootbrugge, M.; De Hosson, J.T.M. Measurement of dispersive forces between evaporated metal surfaces in the range below 100nm. *Appl. Phys. Lett.* **2008**, *92*, 054101. [CrossRef]
36. Tonck, A.; Houze, F.; Boyer, L.; Loubet, J.L.; Georges, J.M. Electrical and mechanical contact between rough gold surfaces in air. *J. Phys. Condens. Matter* **1991**, *3*, 5195. [CrossRef]
37. Sedighi, M.; Svetovoy, V.B.; Palasantzas, G. Casimir force measurements from silicon carbide surfaces. *Phys. Rev. B* **2016**, *93*, 085434. [CrossRef]
38. Van Zwol, P.J.; Palasantzas, G.; De Hosson, J.T.M. Influence of random roughness on the Casimir force at small separations. *Phys. Rev. B* **2008**, *77*, 075412. [CrossRef]
39. Broer, W.; Palasantzas, G.; Knoester, J.; Svetovoy, V.B. Roughness correction to the Casimir force beyond perturbation theory. *EPL* **2011**, *95*, 30001. [CrossRef]
40. Broer, W.; Palasantzas, G.; Knoester, J.; Svetovoy, V.B. Roughness correction to the Casimir force at short separations: Contact distance and extreme value statistics. *Phys. Rev. B* **2012**, *85*, 155410. [CrossRef]
41. Svetovoy, V.; Postnikov, A.; Uvarov, I.; Stepanov, F.; Palasantzas, G. Measuring the Dispersion Forces Near the van der Waals–Casimir Transition. *Phys. Rev. Appl.* **2020**, *13*, 064057. [CrossRef]
42. Svetovoy, V.B.; Melenev, A.E.; Lokhanin, M.V.; Palasantzas, G. Global consequences of a local Casimir force: Adhered cantilever. *Appl. Phys. Lett.* **2017**, *111*, 011603. [CrossRef]
43. Derjaguin, B. Untersuchungen über die Reibung und Adhäsion, IV. *Kolloid-Zeitschrift* **1934**, *69*, 155–164. [CrossRef]
44. Wang, Q.; Chung, Y.W. (Eds.) *Encyclopedia of Tribology*; Springer: Berlin/Heidelberg, Germany, 2013.
45. Goryacheva, I. *Contact Mechanics in Tribology*; Solid Mechanics and Its Applications; Springer: Berlin/Heidelberg, Germany, 1998.
46. Galin, L.; Gladwell, G. *Contact Problems: The Legacy of L.A. Galin*; Solid Mechanics and Its Applications; Springer: Berlin/Heidelberg, Germany, 2008.
47. Muller, V.; Yushchenko, V.; Derjaguin, B. On the influence of molecular forces on the deformation of an elastic sphere and its sticking to a rigid plane. *J. Colloid Interface Sci.* **1980**, *77*, 91–101. [CrossRef]
48. Soldatenkov, I. The use of the method of successive approximations to calculate an elastic contact in the presence of molecular adhesion. *J. Appl. Math. Mech.* **2012**, *76*, 597–603. [CrossRef]
49. Soldatenkov, I. The contact problem with the bulk application of intermolecular interaction forces (a refined formulation). *J. Appl. Math. Mech.* **2013**, *77*, 629–641. [CrossRef]
50. Tas, N.; Sonnenberg, T.; Jansen, H.; Legtenberg, R.; Elwenspoek, M. Stiction in surface micromachining. *J. Micromech. Microeng.* **1996**, *6*, 385–397. [CrossRef]
51. Maboudian, R.; Howe, R.T. Critical Review: Adhesion in surface micromechanical structures. *J. Vac. Sci. Technol. B* **1997**, *15*, 1–20. [CrossRef]
52. Parker, E.E.; Ashurst, W.R.; Carraro, C.; Maboudian, R. Adhesion characteristics of MEMS in microfluidic environments. *J. Microelectromech. Syst.* **2005**, *14*, 947–953. [CrossRef]
53. De Boer, M.P.; Michalske, T.A. Accurate method for determining adhesion of cantilever beams. *J. Appl. Phys.* **1999**, *86*, 817–827. [CrossRef]
54. Van Zwol, P.J.; Svetovoy, V.B.; Palasantzas, G. Distance upon contact: Determination from roughness profile. *Phys. Rev. B* **2009**, *80*, 235401. [CrossRef]
55. Svetovoy, V.B.; van Zwol, P.J.; Palasantzas, G.; De Hosson, J.T.M. Optical properties of gold films and the Casimir force. *Phys. Rev. B* **2008**, *77*, 035439. [CrossRef]
56. Kim, J.Y.; Greer, J.R. Tensile and compressive behavior of gold and molybdenum single crystals at the nano-scale. *Acta Mater.* **2009**, *57*, 5245–5253. [CrossRef]
57. Israelachvili, J.N. *Intermolecular and Surface Forces*; Elsevier: Amsterdam, The Netherlands, 2011.
58. Svetovoy, V.; Palasantzas, G. Influence of surface roughness on dispersion forces. *Adv. Colloid Interface Sci.* **2015**, *216*, 1–19. [CrossRef]
59. Genet, C.; Lambrecht, A.; Neto, P.M.; Reynaud, S. The Casimir force between rough metallic plates. *Europhys. Lett.* **2003**, *62*, 484–490. [CrossRef]
60. Maia Neto, P.A.; Lambrecht, A.; Reynaud, S. Casimir effect with rough metallic mirrors. *Phys. Rev. A* **2005**, *72*, 012115. [CrossRef]
61. Munaò, G.; Correa, A.; Pizzirusso, A.; Milano, G. On the calculation of the potential of mean force between atomistic nanoparticles. *Eur. Phys. J. E* **2018**, *41*, 38. [CrossRef]
62. Gumbel, E.J. *Statistics of Extremes*; Dover: New York, NY, USA, 2004.
63. Palik, E.D. (Ed). *Handbook of Optical Constants of Solids*; Academic Press: New York, NY, USA, 1985.
64. Timoshenko, S.; Goodier, J.N. *Theory of Elasticity*; McGraw-Hill Book Conmpany, Inc.: New York, NY, USA, 1951.
65. Dillard, D.A.; Mukherjee, B.; Karnal, P.; Batra, R.C.; Frechette, J. A review of Winkler's foundation and its profound influence on adhesion and soft matter applications. *Soft Matter* **2018**, *14*, 3669–3683. [CrossRef]
66. Islam, A.A.; Klassen, R.J. Kinetics of length-scale dependent plastic deformation of gold microspheres. *J. Mater. Res.* **2017**, *32*, 3507–3515. [CrossRef]